Available online at www.sciencedirect.com
ScienceDirect
Journal of Organometallic Chemistry 692 (2007) 4535–4544
Journal of Organometallic Chemistry
www.elsevier.com/locate/jorganchem

Remarkable Lewis acid effects on polymerization of functionalized alkenes by metallocene and lithium ester enolates

Yalan Ning, Hongping Zhu, Eugene Y.-X. Chen *

Department of Chemistry, Colorado State University, Fort Collins, CO 80523-1872, United States

Received 11 March 2007; received in revised form 5 May 2007; accepted 6 May 2007
Available online 22 May 2007

Contribution to a special issue dedicating to Prof. Gerhard Erker on the occasion of his 60th birthday.

Abstract

Drastic effects of Lewis acids $E(C_6F_5)_3$ (E = Al, B) on polymerization of functionalized alkenes such as methyl methacrylate (MMA) and *N*,*N*-dimethyl acrylamide (DMAA) mediated by metallocene and lithium ester enolates, $Cp_2Zr[OC(O^iPr)=CMe_2]_2$ (**1**) and $Me_2C=C(O^iPr)OLi$, are documented as well as elucidated. In the case of metallocene bis(ester enolate) **1**, when combined with 2 equiv. of $Al(C_6F_5)_3$, it effects highly active ion-pairing polymerization of MMA and DMAA; the living nature of this polymerization system allows for the synthesis of well-defined diblock and triblock copolymers of MMA with longer-chain alkyl methacrylates. In sharp contrast, the **1**/2B$(C_6F_5)_3$ combination exhibits low to negligible polymerization activity due to the formation of ineffective adduct $Cp_2Zr[OC(O^iPr)=CMe_2]^+[O=C(O^iPr)CMe_2B(C_6F_5)_3]^-$ (**2**). Such a profound Al vs. B Lewis acid effect has also been observed for the lithium ester enolate; while the $Me_2C=C(O^iPr)OLi/2Al(C_6F_5)_3$ system is *highly active* for MMA polymerization, the seemingly analogous $Me_2C=C(O^iPr)OLi/2B(C_6F_5)_3$ system is *inactive*. Structure analyses of the resulting lithium enolaluminate and enolborate adducts, $Li^+[Me_2C=C(O^iPr)OAl(C_6F_5)_3]^-$ (**3**) and $Li^+[Me_2C=C(O^iPr)OB(C_6F_5)_3]^-$ (**4**), coupled with polymerization studies, show that the remarkable differences observed for Al vs. B are due to the inability of the lithium enolborate/borane pair to effect the bimolecular, activated-monomer anionic polymerization as does the lithium enolaluminate/alane pair.

Keywords: Metallocene catalysts; MMA polymerization; Anionic polymerization; Block copolymers; Enolaluminates; Enolborates

1. Introduction

Erker and co-workers [1] first reported facile electrophilic addition of the strongly Lewis acidic $B(C_6F_5)_3$ to nucleophilic group 4 metallocene *ketone enolates*, $Cp_2M[OC(Me)=CH_2]_2$ (M = Ti, Zr, Hf), affording the corresponding mono-adduct $Cp_2M[OC(Me)=CH_2]^+[OC(Me)CH_2B(C_6F_5)_3]^-$ or bis-adduct $Cp_2M^{++}[OC(Me)CH_2B(C_6F_5)_3]_2^-$, depending on the molar equivalents of the added $B(C_6F_5)_3$. Remarkably, this type of adduct formation does not annihilate nucleophilic and electrophilic properties of the adduct constituents. Thus, a combination of $Cp_2M[OC(Me)=CH_2]_2$ with $B(C_6F_5)_3$ is active for polymerization of methyl vinyl ketone with activity of the mixture increasing as the molar equivalent of $B(C_6F_5)_3$ is increased from 1 to 4.

We observed the reaction of chiral *ansa*-zirconocene *ester enolates*, *rac*-(EBI)ZrMe$[OC(O^iPr)=CMe_2]$ and *rac*-(EBI)Zr$[OC(O^iPr)=CMe_2]_2$ [EBI = $C_2H_4(Ind)_2$], with strong Lewis acids $E(C_6F_5)_3$ (E = Al, B) is highly sensitive to both the *ansa*-zirconocene precursor and E; for the methyl zirconocene mono-ester enolate, its reaction with $Al(C_6F_5)_3$ proceeds through a Lewis acid-assisted intramolecular proton transfer process to afford the carboxylate-bridged ion pair $[rac\text{-(EBI)ZrMe}]^+[OC(^iPr)OAl(C_6F_5)_3]^-$ after elimination of propylene, whereas its reaction with $B(C_6F_5)_3$ (in the presence of 1 equiv. of THF as stabilizing

* Corresponding author. Tel.: +1 970 491 5609; fax: +1 970 491 1801.
E-mail address: eychen@lamar.colostate.edu (E.Y.-X. Chen).

0022-328X/$ - see front matter © 2007 Elsevier B.V. All rights reserved.
doi:10.1016/j.jorganchem.2007.05.012

reagent) proceeds through a methide abstraction route to give the cationic ester enolate complex {*rac*-(EBI)Zr^{+}-(THF)[OC(O^{i}Pr)=CMe_2]}[$MeB(C_6F_5)_3$]$^{-}$ [2]. Likewise, the reaction involving the bis(ester enolate) critically hinges on E; although its direct contact with $Al(C_6F_5)_3$ leads to a mixture of products due to decomposition, in the presence of the methyl methacrylate (MMA) monomer the reaction cleanly generates active species that promotes rapid diastereospecific ion-paring polymerization (DIPP) of MMA producing P(MMA) with unique isotactic-*b*-syndiotactic stereo-multiblock microstructures [3]. On the other hand, the reaction of the bis(ester enolate) with 1 or 2 equiv. of $B(C_6F_5)_3$ follows Erker's electrophilic addition pathway generating the cationic zirconocene ester enolate–α-ester borate ion pair *rac*-(EBI)Zr[OC(O^{i}Pr)=CMe_2]$^{+}$[O=C-(O^{i}Pr)$CMe_2B(C_6F_5)_3$]$^{-}$, which is an active catalyst for the production of the structurally controlled P(MMA) having a high isotacticity of [*mm*] = 96% and a narrow molecular weight distribution (MWD) of $M_w/M_n = 1.05$ [3].

We and others have been studying the *controlled* polymerization of functionalized alkenes such as MMA and *N*,*N*-dimethylacrylamide (DMAA) using group 4 metallocene *ester or amide enolate* catalysts incorporating achiral C_{2v} [4], chiral C_2 [2,5] and C_1 [6], as well as prochiral C_s [7] ligand symmetries. Some of these polymerization systems are living and stereospecific, thereby allowing for a high degree of control over the polymer MW, MWD, and stereomicrostructure (tacticity), as well as for the synthesis of well-defined block and stereoblock copolymers. In a closely related work, Erker and co-workers [8] carried out a detailed comparative study of MMA polymerization using a series of *ansa*-zirconocene *dimethyl* and *ansa*-zirconocene *butadiene* precursors varying steric bulk of alkyl substituents at one of the *ansa*-Cp rings, both activated by $B(C_6F_5)_3$ leading to the catalysts having the same cations but different anion structures; this work is significant because it provided direct evidence for the anion effect on the stereoselectivity in the metallocene-catalyzed polymerization of MMA.

Within the ester enolate family, simple lithium ester enolates can also initiate polymerization of MMA, producing, however, ill-defined, multimodal polymers [9]. Significantly, a combination of the lithium ester enolate with 2 equiv. of suitable aluminum Lewis acids, especially $Al(C_6F_5)_3$, promotes *highly active* MMA polymerization and, more importantly, produces P(MMA) with controlled MW and narrow MWD ($M_w/M_n = 1.04$) even at room temperature [9,10]. Unexpectedly, addition of 1 or 2 equiv. of the seemingly analogous $B(C_6F_5)_3$ to the lithium ester enolate *completely halted* the polymerization [9]! Similar observations were also seen for the MMA polymerization mediated by zirconocene imido complexes [6b] as well as aluminum and zinc alkyl complexes [11].

The current contribution examines two unaddressed issues: (a) Lewis acid effects on the MMA polymerization by achiral C_{2v}-metallocene ester enolate Cp_2Zr[OC(O^{i}Pr)=CMe_2]$_2$ and (b) explanations for the already observed extreme Lewis acid effects on the MMA polymerization by lithium ester enolate Me_2C=C(OR)OLi. We found that there exhibit drastic Al vs. B Lewis acid effects on the polymerization activity for both ester enolate systems and subsequently elucidated these effects.

2. Experimental

2.1. Materials and methods

All syntheses and manipulations of air- and moisture-sensitive materials were carried out in flamed Schlenk-type glassware on a dual-manifold Schlenk line, a high-vacuum line, or in an argon or nitrogen-filled glovebox. NMR-scale reactions (typically in a 0.02 mmol scale) were conducted in Teflon-valve-sealed J. Young-type NMR tubes. HPLC grade organic solvents were sparged extensively with nitrogen during filling of the solvent reservoir and then dried by passage through activated alumina (for THF, Et_2O, and CH_2Cl_2) followed by passage through Q-5-supported copper catalyst (for toluene and hexanes) stainless steel columns. Benzene-d_6 and toluene-d_8 were degassed, dried over sodium/potassium alloy, and filtered before use, whereas CD_2Cl_2 was degassed and dried over activated Davison 4 Å molecular sieves. NMR spectra were recorded on a Varian Inova 300 (FT 300 MHz, ^{1}H; 75 MHz, ^{13}C; 282 MHz, ^{19}F), a Varian Inova 400, or a Varian Inova 500 spectrometer. Chemical shifts for ^{1}H and ^{13}C spectra were referenced to internal solvent resonances and are reported as parts per million relative to tetramethylsilane, whereas ^{19}F NMR spectra were referenced to external $CFCl_3$. Elemental analyses were performed by Desert Analytics, Tucson, AZ.

All common reagents were purchased from Aldrich and used as received unless otherwise indicated. Commercially purchased monomers methyl methacrylate (MMA), *n*-butyl methacrylate (BMA) from Alfa Aesar, 2-ethylhexyl methacrylate (EHM) from TCI America, and *N*,*N*-dimethylacrylamide (DMAA) from TCI America were purified by first degassing and drying over CaH_2 overnight, followed by vacuum distillation. Further purification of MMA involved titration with neat tri(*n*-octyl)aluminum to a yellow end point [12] followed by distillation under reduced pressure. The purified monomers were stored in brown bottles over activated Davison 4-Å molecular sieves (for DMAA) in a −30 °C freezer inside the glovebox. Butylated hydroxytoluene (BHT-H, 2,6-di-*tert*-butyl-4-methylphenol) was recrystallized from hexanes prior to use.

Tris(pentafluorophenyl)borane $B(C_6F_5)_3$ was obtained as a research gift from Boulder Scientific Co. and further purified by recrystallization from hexanes at −30 °C. Tris-(pentafluorophenyl)alane $Al(C_6F_5)_3$, as a 0.5 toluene adduct $Al(C_6F_5)_3 \cdot (C_7H_8)_{0.5}$, was prepared by the reaction of $B(C_6F_5)_3$ and $AlMe_3$ in a 1:3 toluene/hexanes solvent mixture in quantitative yield [13]; this is a modified preparation based on literature procedures [14]. Although we have experienced no incidents when handling this material,

extra caution should be exercised, especially when dealing with the unsolvated form, because of its thermal and shock sensitivity. Lithium isopropyl isobutyrate $Me_2C{=}C(O^iPr)$-OLi was prepared according to modified literature procedures [15]; the isolated lithium ester enolate was stored in a freezer at −30 °C inside the glovebox.

2.2. Preparation of $Cp_2Zr[OC(O^iPr){=}CMe_2]_2$ (1)

The literature procedure for the preparation of the methyl derivative, $Cp_2Zr[OC(OMe){=}CMe_2]_2$ [4g], was modified for the preparation of precursor **1**. To a stirred solution of Cp_2ZrCl_2 (0.10 g, 0.34 mmol) in 15 mL of THF at −78 °C was added a solution of $Me_2C{=}C(O^iPr)OLi$ (0.093 g, 0.68 mmol) in 7 mL of THF at −78 °C by cannula. The resulting mixture was gradually warmed to room temperature and stirred for 6 h. The solvent was removed in vacuo, and the resulting suspension was extracted with 20 mL of hexanes inside a glovebox, followed by filtration through a pad of Celite. The yellow filtrate was dried in vacuo to give 0.11 g (67%) of the title product as a yellow oil. ^{1}H NMR (C_6D_6, 21 °C) or $Cp_2Zr[OC(O^iPr){=}CMe_2]_2$ (**1**): δ 6.12 (s, 10H, C_5H_5), 4.27 (sept, $J = 6.3$ Hz, 2H, C*H*Me$_2$), 1.93 (s, 6H, =C*Me*$_2$), 1.78 (s, 6H, =C*Me*$_2$), 1.21 (d, $J = 6.3$ Hz, 12H, CH*Me*$_2$).

2.3. Isolation of $Cp_2Zr[OC(O^iPr){=}CMe_2]^+[O{=}C(O^iPr)$-$CMe_2B(C_6F_5)_3]^-$ (2)

In an argon-filled glovebox, a 20 mL glass reactor was charged with $Cp_2Zr[OC(O^iPr){=}CMe_2]_2$ (0.048 g, 0.10 mmol), $B(C_6F_5)_3$ (0.051 g, 0.10 mmol), and 5 mL of CH_2Cl_2. The resulting orange solution was stirred for 15 min at ambient temperature, after which it was left overnight at −30 °C inside the freezer of the glovebox. The orange red solution was filtrated, and the filtrate was dried in vacuo to give 0.08 g of the title complex (82%) as a red oil; this oily product was not crystallized upon treatment with various types of common crystallization solvents. Anal. Calc. for $C_{42}H_{36}BO_4F_{15}Zr$: C, 50.87; H, 3.66. Found: C, 49.99; H, 3.27%.

^{1}H NMR (CD_2Cl_2, 21 °C) for $Cp_2Zr[OC(O^iPr){=}CMe_2]^+[O{=}C(O^iPr)CMe_2B(C_6F_5)_3]^-$ (**2**): δ 6.60 (s, 10H, C_5H_5), 5.00 (sept, $J = 6.3$ Hz, 1H, C*H*Me$_2$), 4.12 (sept, $J = 6.3$ Hz, 1H, C*H*Me$_2$), 1.70 (s, 3H, =C*Me*$_2$), 1.47 (d, $J = 6.3$ Hz, 6H, OCH*Me*$_2$), 1.42 (br, 6H, C*Me*$_2$), 1.35 (s, 3H, =C*Me*$_2$), 1.24 (d, $J = 6.3$ Hz, 6H, OCH*Me*$_2$). ^{19}F NMR (CD_2Cl_2, 21 °C): δ −132.3 (d, $^3J_{F-F} = 18.3$ Hz, 6F, *o*-F), −163.0 (t, $^3J_{F-F} = 19.7$ Hz, 3F, *p*-F), −165.9 (m, 6F, *m*-F).

2.4. Isolation and structure analysis of $Li^+[Me_2C{=}C$-$(O^iPr)OAl(C_6F_5)_3]^-$ (3) and $Li^+[Me_2C{=}C(O^iPr)OB$-$(C_6F_5)_3]^-$ (4)

In an argon-filled glovebox, a 30 mL glass reactor was charged with $Me_2C{=}C(O^iPr)OLi$ (0.041 g, 0.30 mmol) and 10 mL of toluene. A solution of $E(C_6F_5)_3$ (0.30 mmol) in 10 mL of toluene was carefully layered on top of the lithium ester enolate solution, and the resulting solution mixture was kept at ambient temperature inside the glove box for 1 week, affording complexes **3** or **4** (85%) as colorless crystals which are suitable for X-ray diffraction analysis. Both complexes are insoluble in common NMR solvents, precluding their NMR analysis in solution; however, they were structurally characterized by X-ray diffraction. Anal. Calc. for $C_{50}H_{26}Al_2F_{30}Li_2O_4$ (**3**): C, 45.20; H, 1.97. Found: C, 45.34; H, 2.41%.

The crystals were quickly covered with a layer of Paratone-N oil (Exxon, dried and degassed at 120 °C/10^{-6} Torr for 24 h) after the mother liquors were decanted and then mounted on a thin glass fiber and transferred into the cold nitrogen stream of a Bruker SMART CCD diffractometer. The structures were solved by direct methods and refined using the Bruker SHELXTL program library by full-matrix least-squares on F^2 for all reflections [16]. All non-hydrogen atoms were located by difference Fourier synthesis and refined anisotropically, whereas hydrogen atoms were included geometrically with U_{iso} tied to the U_{iso} of the parent atoms and refined isotropically. Selected crystal data and structural refinement parameters are collected in Table 1.

2.5. General polymerization procedures and polymer characterizations

Polymerizations were performed either in 25-mL flame-dried Schlenk flasks interfaced to the dual-manifold Schlenk line for runs using external temperature bath, or in 20-mL glass reactors inside the glovebox for ambient temperature (~25 °C) runs. In a typical procedure, a predetermined amount of $E(C_6F_5)_3$ was first dissolved in MMA (9.35 mmol) inside a glovebox, and the polymerization was started by rapid addition of the $E(C_6F_5)_3$-MMA solution via gastight syringe to a solution of **1** in 10 mL of CH_2Cl_2 under vigorous stirring at the pre-equilibrated bath temperature. (The amount of MMA was fixed for all polymerizations, whereas the amounts of $E(C_6F_5)_3$ and **1** were adjusted according to the ratios specified in the polymerization tables.) For block copolymerizations, a second quantity of a different monomer was added after the completion of the first block (with the required time indicated in the polymerization table), and the polymerization was continued. After the measured time interval, a 0.2 mL aliquot was taken from the reaction mixture via syringe and quickly quenched into a 4 mL vial containing 0.6 mL of undried "wet" $CDCl_3$ stabilized by 250 ppm of BHT-H; the quenched aliquots were later analyzed by ^{1}H NMR to obtain monomer conversion data. The polymerization was immediately quenched after the removal of the aliquot by the addition of 5 mL 5% HCl-acidified methanol. For MMA and other methacrylate polymerizations, the quenched mixture was precipitated into 100 mL of methanol, stirred for 1 h, filtered, washed with methanol, and

Table 1
Crystal data and structure refinements for **3** (Al) and **4** (B)[a]

	3	**4**
Formula	$C_{50}H_{26}Al_2F_{30}Li_2O_4$	$C_{50}H_{26}B_2F_{30}Li_2O_4$
Formula weight	1328.55	1296.21
Color, habit	Colorless, plate	Colorless, cube
Crystal system	Monoclinic	Monoclinic
Space group	*P*2(1)/*n*	*P*2(1)/*n*
a (Å)	13.1937(10)	12.9476(3)
b (Å)	13.3605(12)	13.2024(3)
c (Å)	15.1332(14)	14.7488(4)
β (°)	95.346(3)	97.851(1)
V (Å^3)	2656.0(4)	2497.5(1)
Z	2	2
ρ_{calc} (g cm^{-3})	1.661	1.721
μ (mm^{-1})	0.205	0.183
F (000)	1320	1288
Crystal size (mm^3)	0.48 × 0.23 × 0.12	0.27 × 0.18 × 0.16
θ Range (°)	1.96–27.48	1.96–32.58
Index Ranges	$-17 \leqslant h \leqslant 17$, $-17 \leqslant k \leqslant 17$, $-19 \leqslant l \leqslant 19$	$-19 \leqslant h \leqslant 12$, $-17 \leqslant k \leqslant 20$, $-22 \leqslant l \leqslant 22$
Collected data	29,575	30,325
Unique data	6053 ($R_{int} = 0.0506$)	9073 ($R_{int} = 0.0606$)
Completeness to *θ* (%)	99.3	100.0
Data/restraints/parameters	6053/0/401	9073/0/401
Goodness-of-fit on F^2	1.012	1.036
Final *R* indices [$I > 2\sigma(I)$]	$R_1 = 0.0454$, $wR_2 = 0.1067$	$R_1 = 0.0617$, $wR_2 = 0.1384$
R indices (all data)	$R_1 = 0.0879$, $wR_2 = 0.1236$	$R_1 = 0.1205$, $wR_2 = 0.1641$
Largest difference if peak and hole/e Å^{-3}	0.334/−0.246	0.521/−0.313

[a] All data were collected at 100(2) K using Mo Kα ($\lambda = 0.71073$ Å) radiation; $R_1 = \sum(||F_o| - |F_c||)/\sum|F_o|$, $wR_2 = \{\sum[w(F_o^2 - F_c^2)^2/\sum[w(F_o^2)^2]\}^{1/2}$; GOF = $\{\sum[w(F_o^2 - F_c^2)^2]/(N_o - N^p)\}^{1/2}$.

dried in a vacuum oven at 50 °C overnight to a constant weight. For DMAA polymerization, the quenched mixture was precipitated into 100 mL of diethyl ether, stirred for 30 min, and the solvent was decanted off. An additional 75 mL of diethyl ether was used to wash the polymer and then decanted; the P(DMAA) product was dried in a vacuum oven at 50 °C to a constant weight.

Glass transition temperatures (T_g) of the polymers were measured by differential scanning calorimetry (DSC) on a DSC 2920, TA Instrument. Samples were first heated to 180 °C at 20 °C/min, equilibrated at this temperature for 4 min, then cooled to −60 °C at 10 °C/min, held at this temperature for 4 min, and reheated to 180 °C at 10 °C/min. All T_g values were obtained from the second scan, after removing the thermal history. Gel permeation chromatography (GPC) analyses of the polymers were carried out at 40 °C and a flow rate of 1.0 mL/min, with $CHCl_3$ as the eluent, on a Waters University 1500 GPC instrument equipped with four 5 μm PL gel columns (Polymer Laboratories) and calibrated using 10 P(MMA) standards. Chromatograms were processed with Waters Empower software (2002); number average molecular weight (M_n) and MWD (M_w/M_n) of polymers are given relative to P(MMA) standards. ^{1}H NMR (300 MHz) spectra of the poly(methacrylate)s and block copolymers were recorded in $CDCl_3$ at room temperature and analyzed according to literature procedures [2,7c,17], whereas ^{13}C NMR (125 MHz) spectra of P(DMAA) were recorded in D_2O at 80 °C and analyzed using literature procedures [5a,18].

3. Results and discussion

3.1. MMA polymerization by $Cp_2Zr[OC(O^iPr)=CMe_2]_2$ (**1**)/$E(C_6F_5)_3$ (E = Al, B)

Control runs using either **1** or $E(C_6F_5)_3$ separately showed no activity for MMA polymerization under the conditions employed in the current study. However, the combination of **1** with 2 equiv. of $Al(C_6F_5)_3$ is highly active for MMA polymerization, achieving a quantitative monomer conversion within just 1 min for the reaction in a $[MMA]_0/[\mathbf{1}]_0$ ratio of 200 (run 1, Table 2). When using CH_2Cl_2 as solvent, it is critical that one follow the polymerization procedures previously established for the

Table 2
Selected MMA polymerization results by **1**/*x*E$(C_6F_5)_3$[a]

Run no.	[Zr] (mM)	$[MMA]_0/[Zr]_0$	Cocation (*x*E)	Time (min)	Conversion[b] (%)	M_n[c] (kg/mol)	MWD[c] (M_w/M_n)	[*mm*][d] (%)	[*mr*][d] (%)	[*rr*][d] (%)
1	4.68	200	2Al	1	100	15.0	1.24	2.1	24.9	73.0
2	2.34	400	2Al	1.5	100	28.8	1.23	2.7	25.2	72.1
3	1.17	800	2Al	150	100	50.4	1.14	2.0	24.3	73.7
4	1.17	800	Al	240	100	52.2	1.14	1.9	24.5	73.6
5	0.78	1200	2Al	690	100	96.6	1.12	1.9	24.7	73.3
6	1.17	800	B	240	9.5	99.1	1.55	4.0	28.0	68.0
7	1.17	800	2B	240	6.4	93.1	1.49	5.1	29.8	65.1

[a] Carried out in a glovebox in 10 mL CH_2Cl_2 at ambient temperature, except for runs 1 and 2 which were performed on a Schlenk line with an external bath set at 25 °C due to large exotherm.
[b] Monomer conversions measured by ^{1}H NMR.
[c] M_n and MWD determined by GPC relative to P(MMA) standards in $CHCl_3$.
[d] Tacticity (methyl triad distribution) determined by ^{1}H NMR.

rac-(EBI)Zr[OC(O^{i}Pr)=CMe$_2$]$_2$/2Al(C$_6$F$_5$)$_3$ system in which Al(C$_6$F$_5$)$_3$ is first mixed (dissolved) in large excess MMA (the amount of which depends on the initial [MMA]$_0$/[**1**]$_0$ ratio employed), followed by addition to a CH_2Cl_2 solution of the zirconocene bis(ester enolate) to start the polymerization [3]. The P(MMA) produced has a syndiotacticity of [*rr*] = 73%, a M_n of 1.50×10^4, and a M_w/M_n of 1.24. As compared to the M_n (calcd) of 1.00×10^4 based on $2[MMA]_0/[I]_0 = 200$, the measured M_n gave an initiator efficiency [$I^* = M_n$(calcd)/M_n(exptl), where M_n(calcd) = MW(MMA) × [MMA]$_0$/[*I*]$_0$ × conversion%] of 67%. This calculation assumed the current system follows the same polymerization mechanism as the *rac*-(EBI)Zr[OC(O^{i}Pr)=CMe$_2$]$_2$/2Al(C$_6$F$_5$)$_3$ system in which approximately two polymer chains are produced per Zr center (i.e., both ester enolate groups initiate the polymerization) [3].

Reducing the amount of [Zr] and [Al] employed by one half while maintaining the [MMA] constant (i.e., [MMA]$_0$/[**1**]$_0$ = 400) still afforded highly active polymerization, achieving a quantitative monomer conversion in 1.5 min (run 2, Table 2). Further increasing the [MMA]$_0$/[**1**]$_0$ ratio required much longer reaction times to achieve the quantitative monomer conversion and, more importantly, effected a nearly linear increase of the resulting polymer M_n, coupled with narrow MWD (Fig. 1). The [Al] concentration also affects polymerization activity (run 3 vs. 4) but *not* the resulting polymer characteristics. All the polymers produced (runs 1–5) have nearly identical syndiotacticity of [*rr*] = 73%, whereas MWD becomes narrower as the polymer M_n gets higher; however, all of them are unimodal, as shown by Fig. 2 which depicts a representative GPC trace of the P(MMA) with $M_n = 9.66 \times 10^4$ and $M_w/M_n = 1.12$ (run 5). Collectively, the evidence discussed above demonstrated the controlled/living characteristics of the polymerization by the **1**/2Al(C$_6$F$_5$)$_3$ system.

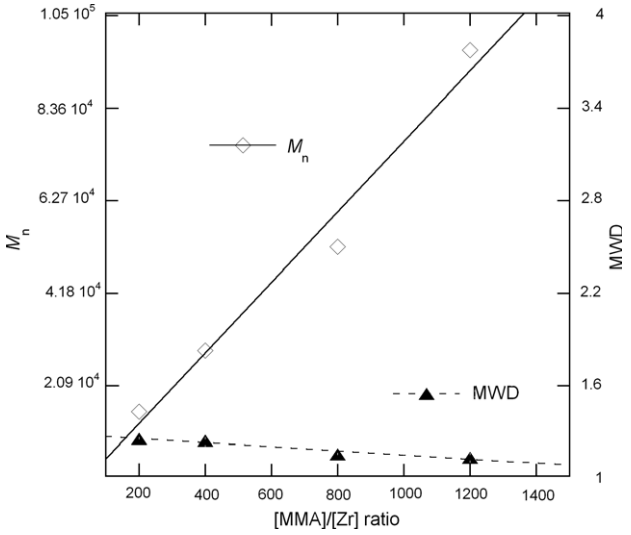

Fig. 1. Plots of M_n and MWD of P(MMA) by **1**/2Al(C$_6$F$_5$)$_3$ vs. the [MAA]$_0$/[**1**]$_0$ ratio.

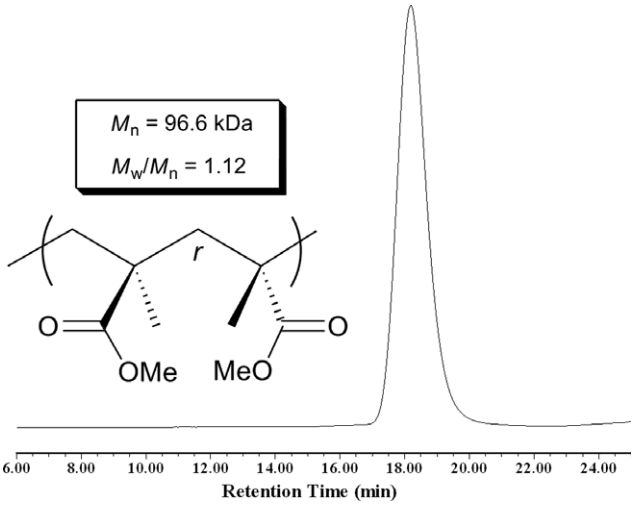

Fig. 2. Representative GPC trace of P(MMA) by **1**/2Al(C$_6$F$_5$)$_3$ (this example is for run 5, Table 2).

Switching the alane Lewis acid to analogous B(C$_6$F$_5$)$_3$ brought about a drastic change in the MMA polymerization behavior. Thus, the **1**/*x*B(C$_6$F$_5$)$_3$ system, regardless of the borane amount ($x = 1$, run 6 vs. $x = 2$, run 7) and the reagent mixing sequence (premixing **1** and the borane followed by addition of MMA vs. premixing the borane and MMA followed by addition to **1**), exhibits low to negligible activity as compared to the **1**/*x*Al(C$_6$F$_5$)$_3$ system. The polymerization achieved only <10% monomer conversions in 4 h and gave high M_n P(MMA), resulting in low I^* of <8% even with a consideration of the production of one polymer chain per Zr center; the polymers have considerably broader MWD and somewhat lower syndiotacticity than those produced by the **1**/*x*Al(C$_6$F$_5$)$_3$ system. The sharp contrast observed for different Lewis acids E(C$_6$F$_5$)$_3$ is attributed to their differences in the activation of the zirconocene bis(ester enolate) and polymerization mechanism (vide infra).

3.2. Methacrylate and acrylamide polymerizations and copolymerizations by **1**/2Al(C$_6$F$_5$)$_3$

As the **1**/2Al(C$_6$F$_5$)$_3$ system shows high activity and also living characteristics in the MMA polymerization, we further employed this superior system for polymerization of other methacrylates (BMA, *n*-butyl methacrylate; EHM, 2-ethylhexyl methacrylate) and an acrylamide (DMAA, *N*,*N*-dimethyl acrylamide), as well as block copolymerization of MMA with BMA and EHM. The purposes of this study are to further explore the utilities of this polymerization system in the production of unique block copolymers and confirm the livingness of the **1**/2Al(C$_6$F$_5$)$_3$ system. Table 3 summarizes the results of this study.

As can be seen from the table, polymerization of BMA proceeds rapidly, achieving a quantitative monomer conversion in 10 min for the reaction using a [BMA]$_0$/[**1**]$_0$ ratio of 400 (run 1, Table 3). The P(BMA) produced

Table 3
(Co)polymerization of methacrylate and acrylamide monomers by **1**/2Al(C_6F_5)$_3$[a]

Run no.	10^2[M]$_0$/[Zr]$_0$ monomer	Time (min)	M_n (kg/mol)	MWD (M_w/M_n)	[*mm*] (%)[b]	[*mr*] (%)[b]	[*rr*] (%)[b]
1	4BMA	10	36.8	1.19	3.1	11.8	85.1
2	4MMA/4BMA	1.5/18.5	59.9	1.37	3.0	12.6	84.4
3	4DMAA	3	36.3	1.16	11.2	26.5	62.3
4	4EHM	60	36.3	1.12	0	11.2	88.8
5	4MMA/4EHM	1.5/18.5	50.0	1.15	0	22.1	77.9
6	4MMA/4EHM/4MMA	1.5/18.5/25	74.0	1.19	0	20.2	79.8

[a] Carried out in 10 mL CH_2Cl_2 at ambient temperature in water bath set at 25 °C; [Zr]$_0$ = 2.34 mM; 100% monomer conversion (by NMR) was achieved for all runs at the indicated reaction time; runs 2, 5, and 6 were sequential diblock, diblock, and triblock copolymerizations, respectively.
[b] Triad distributions in the methyl region for poly(methacrylate)s and in the C=O region for P(DMAA) were determined by ^{1}H NMR (300 MHz) in $CDCl_3$ at RT and ^{13}C NMR (125 MHz) in D_2O at 80 °C, respectively.

has a syndiotacticity of [*rr*] = 85%, a M_n of 3.68×10^4, and a MWD of $M_w/M_n = 1.19$; the calculated I^* is 77% for the production of two polymer chains per Zr center. Sequential copolymerization of MMA and BMA starting from polymerization of MMA afforded diblock copolymer P(MMA)-*b*-P(BMA), with the final M_n nearing the sum of two homopolymers (run 2, Table 3). The **1**/2Al(C_6F_5)$_3$ system is also highly active for DMAA polymerization, converting all 400 equiv. of DMAA to the well-defined P(DMAA) ($M_w/M_n = 1.16$) in 3 min (run 3, Table 3). The T_g of P(DMAA) is 122 °C, consistent with its syndio-rich atactic stereomicrostructure [18a].

Long-chain alkyl methacrylate EHM was also effectively polymerized by **1**/2Al(C_6F_5)$_3$ to the unimodal, syndiotactic P(EHM) with $M_w/M_n = 1.12$ and [*rr*] = 89% (run 4, Table 3). Sequential copolymerizations of MMA and EHM afforded well-defined diblock copolymer P(MMA)-*b*-P(EHM) (run 5) and triblock copolymer P(MMA)-*b*-P(EHM)-*b*-P(MMA) (run 6). The block copolymers produced are unimodal and exhibit narrow MWD with the final M_n increased approximately according to the sum of the block components (Fig. 3). The diblock copolymer exhibits two distinct T_g's characteristic of each of the component segments [i.e,

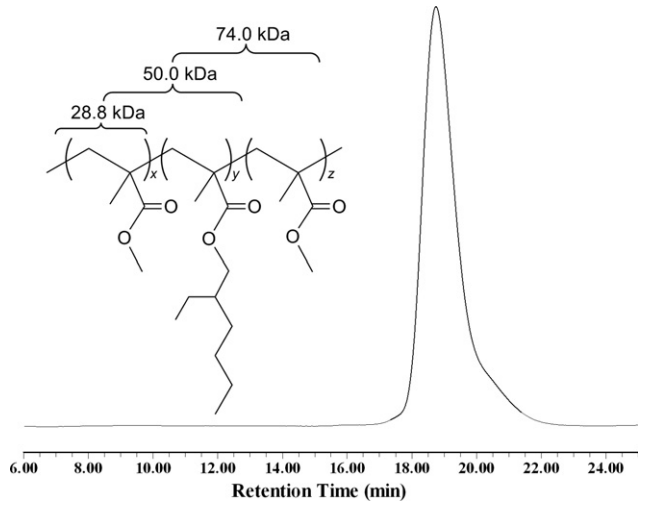

Fig. 3. GPC trace of triblock copolymer P(MMA)-*b*-P(EHM)-*b*-P(MMA) produced by the **1**/2Al(C_6F_5)$_3$ system ($M_n = 7.40 \times 10^4$, $M_w/M_n = 1.19$ for run 6 in Table 3).

$T_g(1) = 133$ °C for the syndiotactic P(MMA) block and $T_g(2) = -4$ °C for the syndiotactic P(EHM) block].

3.3. Activation of zirconocene bis(ester enolate) (*1*) by $E(C_6F_5)_3$

We have previously examined in detail all the possible elementary reactions involved in the MMA polymerization by *rac*-(EBI)Zr[OC(O^{i}Pr)=CMe$_2$]$_2$/2Al(C_6F_5)$_3$ [3]. Direct contact of the zirconocene bis(enolate) with Al(C_6F_5)$_3$ leads to a mixture of products due to decomposition. However, in the polymerization procedure we employed (vide supra) at no time does the free Al(C_6F_5)$_3$ exist because it is always in the form of an adduct with either MMA or the ester group of the polymer chain. Thus, the relevant reaction to consider is the reaction of the zirconocene bis(enolate) with the adduct Al(C_6F_5)$_3$ · MMA. In short, that comprehensive study concluded that the polymerization by *rac*-(EBI)Zr[OC(O^{i}Pr)=CMe$_2$]$_2$/2Al(C_6F_5)$_3$ produces P(MMA) with isotactic-*b*-syndiotactic stereo-multiblock microstructures, proceeding through a unique diastereospecific ion-paring polymerization mechanism which consists of four manifolds—an isospecific cycle by the chiral zirconocene cation, a syndiospecific cycle by the enolaluminate anion, anion-monomer exchange, and then chain transfer, the latter two serving to interconvert diastereospecific propagating manifolds [3]. It is assumed that the current, analogous Cp$_2$Zr[OC(O^{i}Pr)=CMe$_2$]$_2$/2Al(C_6F_5)$_3$ system follows the same activation and MMA polymerization pathways as the *rac*-(EBI)Zr[OC(O^{i}Pr)=CMe$_2$]$_2$/2Al(C_6F_5)$_3$ system, involving ion-pairing active propagating species consisting of Cp$_2$Zr[(OC(OMe)=C(Me)P)]$^+$ and [P(Me)C=C(OMe)OAl(C_6F_5)$_3$]$^-$ (Scheme 1, where P denotes a growing polymer chain and only the bimetallic propagation manifold is shown). Because the current system employs the achiral C_{2v}-symmetric zirconocene ester enolate, both cationic zirconocene ester enolate and anionic enolaluminate sites are syndioselective by a chain-end control mechanism in the ion-pairing polymerization of MMA, thereby producing P(MMA) with predominately syndiotactic microstructures.

The substantial Al vs. B differences observed in the MMA polymerization by the **1**/*x*E(C_6F_5)$_3$ system were also seen for the chiral *rac*-(EBI)Zr[OC(O^{i}Pr)=CMe$_2$]$_2$/

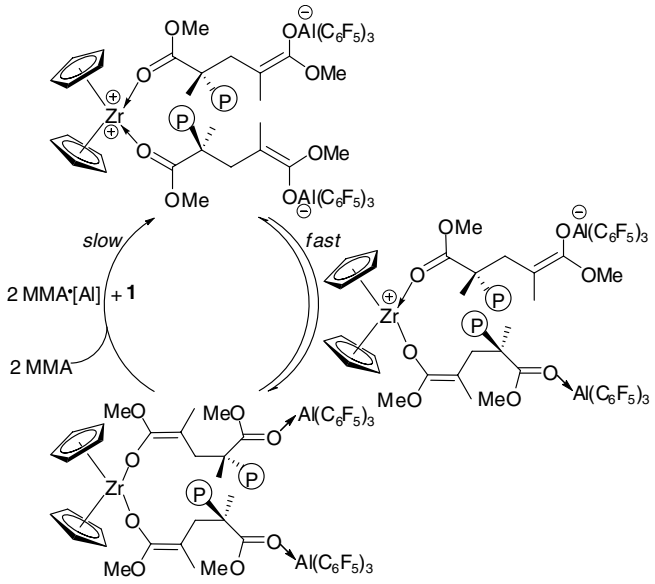

Scheme 1.

xE(C_6F_5)$_3$ system [3]. As in the latter chiral system, the reaction of achiral **1** with 1 equiv. of B(C_6F_5)$_3$ forms cationic zirconocene ester enolate–α-ester borate ion pair $Cp_2Zr[OC(O^iPr)=CMe_2]^+[O=C(O^iPr)CMe_2B(C_6F_5)_3]^-$ (**2**, Scheme 2), derived from apparent electrophilic addition of the borane to the nucleophilic ester enolate α-carbon, reminiscent of the reaction of B(C_6F_5)$_3$ with the sterically unprotected bis(2-propenolato)zirconocene reported by Erker et al. [1]. The ^{19}F NMR (CD_2Cl_2) chemical shifts of −132.3 (d, 6F, *o*-F), −163.0 (t, 3F, *p*-F), −165.9 (m, 6F, *m*-F) for the α-ester borate anion in **2** are identical to those observed for the same anion but paired with the chiral cation *rac*-(EBI)Zr[OC(O^{i}Pr)=CMe$_2$]$^+$. Consistent with the transformation of one ester enolate ligand in **1** to the ester group in **2** upon treatment with B(C_6F_5)$_3$, the ^{1}H NMR signal for the methine proton in –C*H*Me$_2$ (sept, 4.27 ppm) attached to the *enolate ligand* in **1** is substantially downfield shifted to 5.00 ppm (sept) for –C*H*Me$_2$ now attached to the *ester group* in **2** [5b], whereas the ^{1}H NMR signal for –C*H*Me$_2$ in the other enolate ligand experienced only a minor shift to 4.12 ppm accounting for the neutral to cationic structural change. The reaction with 2 equiv. of B(C_6F_5)$_3$ affords the same product with no indication for the formation of the possible bis-adduct. Hence, the species derived from the borane activation is active only at the cationic site, while the ester borate anion is inactive for the MMA polymerization.

The observed little activity for the cation portion of **2** is consistent with prior findings that the cationic zirconocene species incorporating non-bridged bis-Cp ligands exhibit low activity in a monometallic polymerization system [4]. Polymerizations by *in situ* mixing of MMA with 1 or 2 equiv. of B(C_6F_5)$_3$ followed by addition of complex **1** (i.e., activated-monomer approach), or by *in situ* mixing of complex **1** with B(C_6F_5)$_3$ followed by addition of MMA (i.e., activated complex approach), afforded similar polymerization results. Overall, the Lewis acid in the **1**/B(C_6F_5)$_3$ system functions only as a cation-forming agent, and neither the resulting anion nor the neutral borane participates in the polymer chain formation steps (Scheme 2) as do Al(C_6F_5)$_3$ and its derived anions in the **1**/Al(C_6F_5)$_3$ system (Scheme 1).

3.4. Structures of lithium ester enolate and E(C_6F_5)$_3$ adducts

As we showed earlier, addition of 1 or 2 equiv. of B(C_6F_5)$_3$ to the lithium ester enolate *completely halted* MMA polymerization [9], whereas the combination of the lithium ester enolate with 2 equiv. of Al(C_6F_5)$_3$ promotes *highly active* MMA polymerization and, more importantly, produces P(MMA) with controlled MW and narrow MWD [9,10]. To seek for a solution to this puzzle, we investigated the reactions of the lithium ester enolate Me$_2$C=C(O^{i}Pr)OLi with E(C_6F_5)$_3$ and structurally characterized the resulting lithium enolaluminate $Li^+[Me_2C=C(O^iPr)OAl(C_6F_5)_3]^-$ (**3**) and enolborate $Li^+[Me_2C=C(O^iPr)OB(C_6F_5)_3]^-$ (**4**).

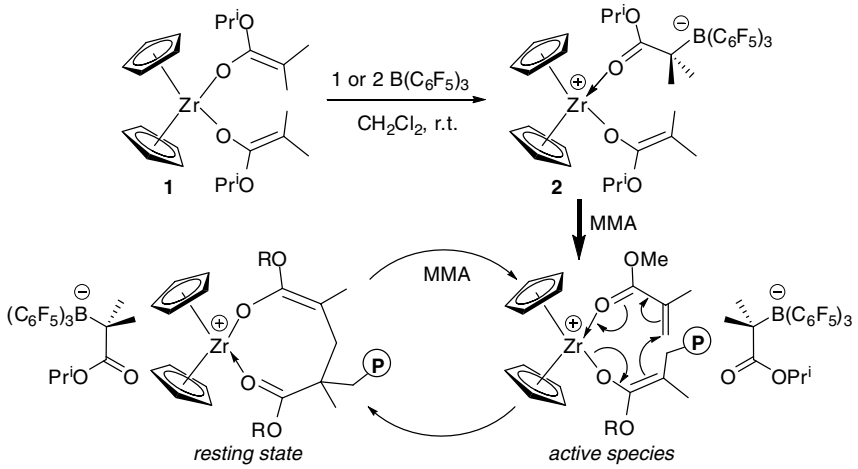

Scheme 2.

The molecular structure of **3** was determined by X-ray diffraction (Fig. 4), featuring a centrosymmetric dimeric structure in the solid state. The two unique lithium enolaluminate $Li^+[Me_2C{=}C(O^iPr)OAl(C_6F_5)_3]^-$ molecules in the dimer are connected by two ionic Li–O_{alkoxy} bonds, presenting a $Li_2O_4C_2$ crown-type eight-membered-ring core linkage where the Li–O_{alkoxy} bond is only slightly shorter than the Li–$O_{enolate}$ bond and the C–O_{alkoxy} bond is slightly longer than the C–$O_{enolate}$ bond, both by ~0.03 Å. The $Al(C_6F_5)_3$ moiety is directly bonded to the enolate oxygen, and the Al center adopts a distorted tetrahedral geometry with a sum of the C–Al–C angles of 336.8°. The Al–O distance [1.784(2) Å] in **3** is noticeably shorter than that [1.820(3) Å] in the *only other structurally characterized lithium enolaluminate* $Li^+[Me_2C{=}C(O^iPr)$-$OAlMe(BHT)_2]^-$ [10], coupled with the smaller Al–O–C vector angle, indicative of a stronger Al–O σ bond in **3**. The coordination sphere of Li^+ is completed by one enolate O, one centrosymmetrically operated alkoxy O, and two *ortho*-F atoms from two different C_6F_5 rings. The C(1)–O(1) [1.367(3) Å], C(1)–O(2) [1.393(3) Å], and C(1)–C(2) [1.322(3) Å] bond lengths evidence a structural feature of the enolate $Me_2C{=}C(O^iPr)O$ moiety where π electron conjugation over these bonds is implied. The enolate and isopropoxy oxygens adopt nearly planar and planar geometries, with the sums of the angles around O(1) and O(2) being 358.9° and 360.0°, respectively. Owing to ionic Li–F interactions with separations of 1.942(4) and 1.992(4) Å, the two Al–C(pentafluoroaryl) bond distances [2.005(2) and 2.003(3) Å] appear slightly (by ~0.02 Å) longer than the third one without such interactions [1.988(2) Å].

The overall structure of lithium enolborate **4** shown in Fig. 5 is remarkably similar to that of lithium enolaluminate **3**. While stronger ionic Li–F interactions are observed in **4**, as evidenced by noticeably shorter Li–F separations in **4** than those observed in **3** (by ~0.05 Å), other metric differences can be accounted by the differences in Al/B covalent radii. The overlay plot of the unique molecules of **3** and **4** depicted in Fig. 6 further shows the striking similarities between these two structures.

Subsequently, we examined the polymerization activity of the isolated lithium enolaluminate **3** and enolborate **4** under identical conditions and found that neither of them showed any activity for MMA polymerization. A striking difference arises when a second equivalent of $E(C_6F_5)_3$ is added: while the **3**/$Al(C_6F_5)_3$ combination [which can also

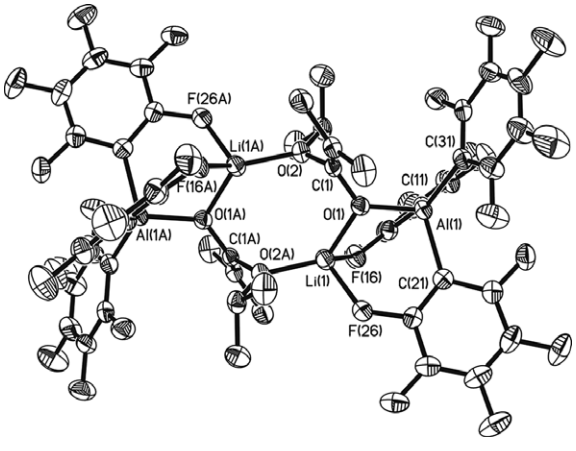

Fig. 4. X-ray crystal structure of **3** with thermal ellipsoids drawn at the 50% probability. Selected bond lengths [Å] and angels [°]: Al(1)–O(1) 1.784(2), Al(1)–C(11) 2.005(2), Al(1)–C(21) 2.003(2), Al(1)–C(31) 1.988(2), Li(1)–O(1) 1.900(4), Li(1)–O(2A) 1.875(4), Li(1)–F(16) 1.992(4), Li(1)–F(26) 1.942(4); C(11)–Al(1)–C(21) 105.0(1), C(11)–Al(1)–C(31) 117.8(1), C(21)–Al(1)–C(31) 114.0(1), Al(1)–O(1)–C(1) 130.4(1), Al(1)–O(1)–Li(1) 111.8(1), C(1)–O(1)–Li(1) 116.6(2).

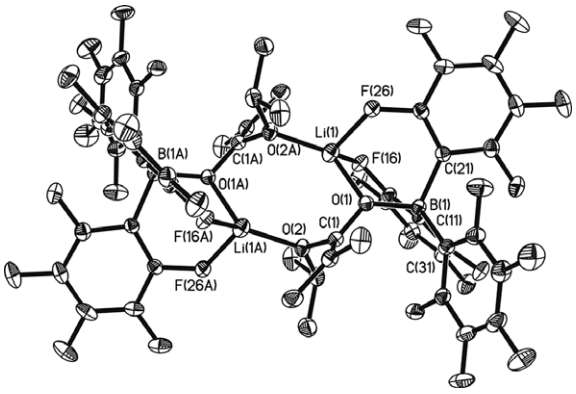

Fig. 5. X-ray crystal structure of **4** with thermal ellipsoids drawn at the 50% probability. Selected bond lengths [Å] and angels [°]: B(1)–O(1) 1.541(3), B(1)–C(11) 1.666(3), B(1)–C(21) 1.650(3), B(1)–C(31) 1.640(3), Li(1)–O(1) 1.880(4), Li(1)–O(2A) 1.886(4), Li(1)–F(16) 1.941(4), Li(1)–F(26) 1.904(4); C(11)–B(1)–C(21) 104.3(2), C(11)–B(1)–C(31) 115.8(2), C(21)–B(1)–C(31) 112.0(2), B(1)–O(1)–C(1) 128.3(2), B(1)–O(1)–Li(1) 118.4(2), C(1)–O(1)–Li(1) 109.2(2).

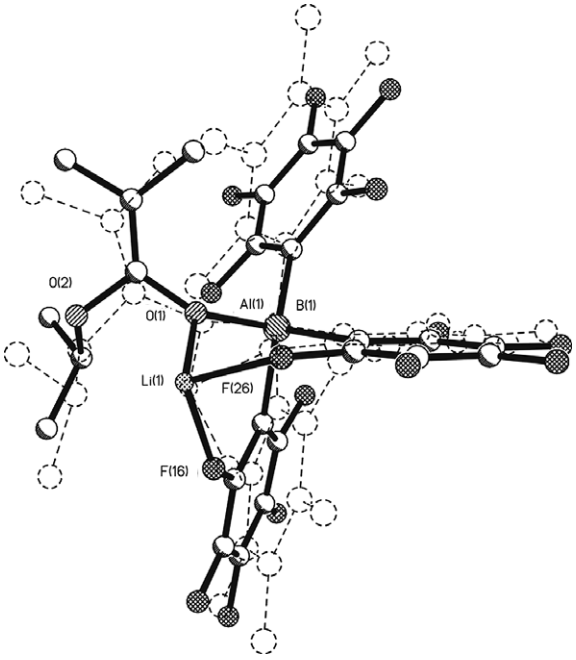

Fig. 6. Overlay plot of the unique molecules of **3** (solid lines) and **4** (dash lines).

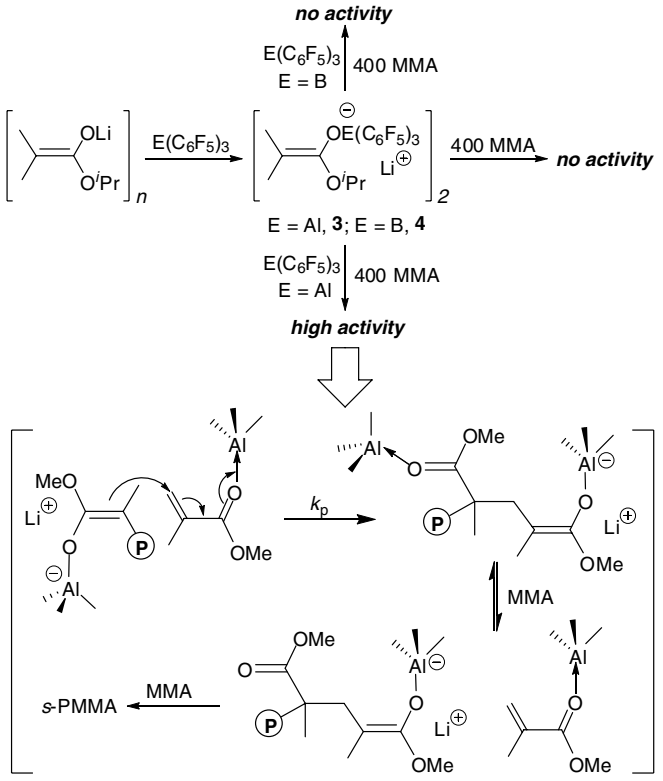

Scheme 3.

be conveniently generated by in situ mixing of $Me_2C{=}C(O^iPr)OLi$ with 2 equiv. of $Al(C_6F_5)_3$] is *highly active* for MMA polymerization, the $\mathbf{4}/B(C_6F_5)_3$ system [or $Me_2C{=}C(O^iPr)OLi/2B(C_6F_5)_3$] is *inactive* (Scheme 3). Collectively, the above structural analysis and polymerization study clearly indicate that the remarkable differences observed for Al vs. B are due to the inability of the lithium enolborate/borane pair to effect the bimolecular, activated-monomer anionic polymerization as does the lithium enolaluminate/alane pair (Scheme 3) [9,10].

4. Conclusions

We presented here two extreme cases of Lewis acid effects on the polymerization of methacrylate and acrylamide monomers by the combination of $E(C_6F_5)_3$ with metallocene and lithium ester enolates, $Cp_2Zr[OC(O^iPr){=}CMe_2]_2$ (**1**) and $Me_2C{=}C(O^iPr)OLi$. In sharp contrast to the low to negligible polymerization activity and ill-behaved polymerization observed for the $\mathbf{1}/xB(C_6F_5)_3$ ($x = 1$, 2) system, the $\mathbf{1}/xAl(C_6F_5)_3$ system is not only highly active but also living in the polymerization of MMA, thereby enabling the synthesis of the well-defined diblock and triblock copolymers including P(MMA)-*b*-P(BMA), P(MMA)-*b*-P(EHM), and P(MMA)-*b*-P(EHM)-*b*-P(MMA). The striking Al vs. B differences observed for the $\mathbf{1}/2E(C_6F_5)_3$ systems are attributed to the facile ion-pairing polymerization via active propagating species consisting of $Cp_2Zr[(OC(OMe){=}C(Me)P)]^+$ and $[P(Me)C{=}C(OMe)OAl(C_6F_5)_3]^-$ enabled by $\mathbf{1}/2Al(C_6F_5)_3$ and the formation of the ineffective cationic zirconocene ester enolate–α-esterborate ion pair $Cp_2Zr[OC(O^iPr){=}CMe_2]^+[O{=}C(O^iPr)\,CMe_2\text{-}B(C_6F_5)_3]^-$ (**2**) derived from $\mathbf{1}/xB(C_6F_5)_3$.

An additional example of such a profound Al vs. B effect in the polymerization of MMA has also been observed for the combination of the lithium ester enolate initiator with Lewis acids $E(C_6F_5)_3$. Again, $Al(C_6F_5)_3$ in the $Me_2C{=}C(O^iPr)OLi/2Al(C_6F_5)_3$ system promotes highly active MMA polymerization, whereas the seemingly analogous $Me_2C{=}C(O^iPr)OLi/2B(C_6F_5)_3$ system is inactive. We structurally characterized the resulting adducts, lithium enolaluminate $Li^+[Me_2C{=}C(O^iPr)OAl(C_6F_5)_3]^-$ (**3**) and enolborate $Li^+[Me_2C{=}C(O^iPr)OB(C_6F_5)_3]^-$ (**4**), and found that they have remarkably similar solid state structures. Overall, the combined structural analyses and the polymerization studies indicate that the extreme differences observed for Al vs. B are due to the inability of the lithium enolborate/borane pair to effect the bimolecular, activated-monomer anionic polymerization as does the lithium enolaluminate/alane pair.

Acknowledgements

Funding for this work was provided by the National Science Foundation. We thank Susie Miller for the X-ray diffraction data collections and Boulder Scientific Co. for the gift of $B(C_6F_5)_3$.

Appendix A. Supplementary material

CCDC 639263 and 639264 contain the supplementary crystallographic data for **3** and **4**. These data can be obtained free of charge via http://www.ccdc.cam.ac.uk/conts/retrieving.html, or from the Cambridge Crystallographic Data Centre, 12 Union Road, Cambridge CB2 1EZ, UK; fax: (+44) 1223-336-033; or e-mail: deposit@ccdc.cam.ac.uk. Supplementary data associated with this article can be found, in the online version, at doi:10.1016/j.jorganchem.2007.05.012.

References

[1] W. Spaether, K. Klaß, G. Erker, F. Zippel, R. Fröhlich, Chem. Eur. J. 4 (1998) 1411–1417.
[2] A.D. Bolig, E.Y.-X. Chen, J. Am. Chem. Soc. 126 (2004) 4897–4906.
[3] Y. Ning, E.Y.-X. Chen, Macromolecules 39 (2006) 7204–7215.
[4] (a) B. Lian, C.W. Lehmann, C. Navarro, J.-F. Carpentier, Organometallics 24 (2005) 2466–2472;
(b) G. Stojcevic, H. Kim, N.J. Taylor, T.B. Marder, S. Collins, S. Angew, Chem. Int. Ed. 43 (2004) 5523–5526;
(c) M. Ferenz, F. Bandermann, R. Sustmann, W. Sicking, Macromol. Chem. Phys. 205 (2004) 1196–1205;
(d) B. Lian, L. Toupet, J.-F. Carpentier, Chem. Eur. J. 10 (2004) 4301–4307;
(e) A.D. Bolig, E.Y.-X. Chen, J. Am. Chem. Soc. 124 (2002) 5612–5613;
(f) F. Bandermann, M. Ferenz, R. Sustmann, W. Sicking, Macromol. Symp. 174 (2001) 247–253;

(g) Y. Li, D.G. Ward, S.S. Reddy, S. Collins, Macromolecules 30 (1997) 1875–1883.
[5] (a) W.R. Mariott, E.Y.-X. Chen, Macromolecules 38 (2005) 6822–6832;
(b) A. Rodriguez-Delgado, E.Y.-X. Chen, Macromolecules 38 (2005) 2587–2594.
[6] (a) J. Jin, W.R. Mariott, E.Y.-X. Chen, J. Polym. Chem. Part A: Polym. Chem. 41 (2003) 3132–3142;
(b) J. Jin, E.Y.-X. Chen, Organometallics 21 (2002) 13–15.
[7] (a) B. Lian, C.M. Thomas, C. Navarro, J.-F. Carpentier, Organometallics 26 (2007) 187–195;
(b) A. Rodriguez-Delgado, W.R. Mariott, E.Y.-X. Chen, J. Organomet. Chem. 691 (2006) 3490–3497;
(c) A. Rodriguez-Delgado, W.R. Mariott, E.Y.-X. Chen, Macromolecules 37 (2004) 3092–3100;
(d) H. Nguyen, A.P. Jarvis, M.J.G. Lesley, W.M. Kelly, S.S. Reddy, N.J. Taylor, S. Collins, Macromolecules 33 (2000) 1508–1510.
[8] J.W. Strauch, J.-L. Fauré, S. Bredeau, C. Wang, G. Kehr, R. Fröhlich, H. Luftmann, G. Erker, J. Am. Chem. Soc. 126 (2004) 2089–2104.
[9] A.D. Bolig, E.Y.-X. Chen, J. Am. Chem. Soc. 123 (2001) 7943–7944.
[10] A. Rodriguez-Delgado, E.Y.-X. Chen, J. Am. Chem. Soc. 127 (2005) 961–974.
[11] D. Chakraborty, E.Y.-X. Chen, Organometallics 22 (2003) 769–774.
[12] R.D. Allen, T.E. Long, J.E. McGrath, Polym. Bull. 15 (1986) 127–134.
[13] S. Feng, G.R. Roof, E.Y.-X. Chen, Organometallics 21 (2002) 832–839.
[14] (a) C.H. Lee, S.J. Lee, J.W. Park, K.H. Kim, B.Y. Lee, J.S. Oh, J. Mol. Cat., A: Chem. 132 (1998) 231–239;
(b) P. Biagini, G. Lugli, L. Abis, P. Andreussi, U.S. Patent 5,602,269 (1997).
[15] Y.-J. Kim, M.P. Bernstein, A.S. Galiano Roth, F.E. Romesberg, P.G. Williard, D.J. Fuller, A.T. Harrison, D.B. Collum, J. Org. Chem. 56 (1991) 4435–4439.
[16] SHELXTL, Version 6.12; Bruker Analytical X-ray Solutions: Madison, WI, 2001.
[17] R.C. Ferguson, D.W. Ovenall, Macromolecules 20 (1987) 1245–1248.
[18] (a) W.R. Mariott, E.Y.-X. Chen, Macromolecules 37 (2004) 4741–4743;
(b) M. Kobayashi, S. Okuyama, T. Ishizone, S. Nakahama, Macromolecules 32 (1999) 6466–6477;
(c) X. Xie, T.E. Hogen-Esch, Macromolecules 29 (1996) 1746–1752;
(d) A. Bulai, M.L. Jimeno, A.-A.A. de Queiroz, A. Gallardo, J.S. Roman, Macromolecules 29 (1996) 3240–3246.